

# Quantum Vibrational Relativity (QVR): A Unified Framework Bridging General Relativity, Quantum Mechanics, and Cosmology

Meena Rajendran 

Independent Theoretical Physicist

[writetome@meenalive.com](mailto:writetome@meenalive.com)

March 2026, Version 2

## Abstract

This paper presents Quantum Vibrational Relativity (QVR), a scalar-field extension of General Relativity in which a single k-essence field with conformal coupling to matter replaces both dark matter particles and a separate cosmological constant. The field's kinetic function  $F(Y) = Y + \frac{2}{3}Y^{3/2}\exp(\lambda Y)$  produces a natural phase transition: during the matter-dominated era, the field freezes into pressureless dust ( $w \rightarrow 0$ ,  $c_s^2 \rightarrow 0$ ), clustering gravitationally to produce the CMB acoustic peaks; at late times, the field transitions into a MOND-like modification of gravity that explains galactic rotation curves without dark matter particles.

We validate this framework against seven independent tests spanning twelve orders of magnitude in energy scale: (1) cosmological–galactic unification  $\kappa = 1.063$  (95% CI [0.908, 1.200]); (2) a  $3.5\sigma$  periodic oscillation in Pantheon+ supernovae; (3) an inelastic coupling mechanism for wavefunction localization; (4) a best-in-class fit to the Galactic Center Excess ( $E_{\text{pk}} = 4.60$  GeV,  $\Delta\text{AIC} = -16.3$ ); (5) null photon dispersion confirming Lorentz invariance; (6) SVEA derivation confirmed with  $L_2$  error below 4%; and (7) CMB acoustic peak positions within 1.5% of Planck and peak height ratios within 4.4%, from a Boltzmann-code implementation with no dark matter particles.

The framework has two physically meaningful parameters ( $\alpha = 1/6$  from galactic self-consistency,  $\lambda \approx 75$  from the CMB), passes all precision tests by large margins ( $c_T = c$  exactly, Cassini by  $10^{11}\times$ , binary pulsars by  $10^{22}\times$ , BBN by  $10^3\times$ , wide binaries at  $0.3\sigma$ ), and makes falsifiable predictions including redshift-dependent  $a_0(z) \propto H(z)$  testable with JWST.

*Keywords:* Quantum gravity; dark matter; dark energy; unified field theory; MOND; k-essence; CMB; Galactic Center Excess; JWST; wide binaries

## 1 Introduction

The standard description of the universe rests on two theoretically incompatible pillars, General Relativity and Quantum Mechanics, supplemented by a concordance cosmology

( $\Lambda$ CDM) in which approximately 95% of the energy content consists of substances that have never been directly detected [1, 2, 3]. Dark matter particles have been sought for four decades in direct detection experiments, at particle colliders, and through indirect astrophysical signals. None have been found. Dark energy remains a placeholder label for the accelerating expansion, with no agreed-upon physical mechanism.

Meanwhile, a persistent empirical regularity challenges the dark matter paradigm: the dynamics of galaxies are governed by a universal acceleration scale  $a_0 \approx 1.2 \times 10^{-10} \text{ m s}^{-2}$ , first identified by Milgrom [4] and confirmed across 175 galaxies in the SPARC database [5, 6]. The near-coincidence  $a_0 \sim cH_0$  has been noted since Milgrom’s original work but has never been derived from a relativistic field theory.

This paper presents a resolution. We show that a single scalar field, added to General Relativity with a specific non-linear kinetic term and a weak conformal coupling to matter, produces all three of the phenomena conventionally attributed to dark matter, dark energy, and modified gravity, and does so from one equation. In its pure form, the scalar field replaces dark matter particles entirely; the current Boltzmann-code implementation achieves 95.6% concordance with Planck CMB data. We identify the computational improvements needed to close the remaining 4.4%, and discuss the possibility that a small residual dark matter fraction may reflect genuine physics rather than numerical limitation.

## 2 The Mechanism: One Field, Three Roles

Before presenting the mathematics, we describe in plain language what the QVR scalar field does and how a single entity can play three apparently distinct roles.

**The field is a cosmic vibration.** Imagine a vibrational field that permeates all of spacetime. In the early universe, when matter is dense, this field vibrates rigidly and uniformly: it has no internal pressure, so it clumps under gravity exactly like the hypothetical cold dark matter particles. It falls into gravitational wells, amplifies the density contrasts that seed galaxy formation, and imprints the acoustic peaks observed in the cosmic microwave background.

**The field’s vibration shifts as the universe expands.** As the matter density drops and the universe approaches the present epoch, the field undergoes a vibrational phase transition. Its oscillation mode changes from rigid and uniform (pressureless, clumping) to fluid and responsive (pressure-bearing, smooth). In this new mode, the field behaves like a repulsive energy, what we call dark energy and the universe’s expansion accelerates.

**In galaxies, the field amplifies gravity.** On galactic scales today, the same field produces an effective gravitational enhancement, amplifying the pull on visible matter to match what would otherwise require a dark matter halo. The field does not need to be the missing mass; it amplifies the existing mass to produce the observed dynamics. This modified gravity follows the MOND phenomenology that Milgrom identified in 1983, with the acceleration scale  $a_0$  set by the cosmological expansion rate:  $a_0(t) = (c/6) H(t)$ .

**One transition, not three phenomena.** Dark matter, dark energy, and MOND are not three separate substances or modifications. They are the same field at three different epochs of its evolution. The CMB acoustic peaks are the harmonic footprint of this field resonating with ordinary matter in the early universe. Galaxy rotation curves are its low-frequency mode today. The accelerating expansion is its vacuum state.

The mathematical engine that produces this behavior is a specific non-linear kinetic function  $F(Y)$  for the scalar field, combined with a weak coupling to matter. The kinetic variable  $Y$  tracks the field’s activity: large  $Y$  in the early universe (dust mode), small  $Y$  today (MOND mode), zero  $Y$  during radiation domination (invisible). The phase transition between these regimes is smooth, analytic, and controlled by a single parameter  $\lambda$  that is determined by the CMB data.

The kinetic variable  $Y$  measures the field’s vibrational intensity: the field’s name reflects this central role of vibration in determining which physical regime—dark matter, dark energy, or modified gravity—manifests at any given epoch.

### 3 The QVR Lagrangian

The complete QVR theory is defined by a single action. We add a scalar field  $\phi$  to the Einstein–Hilbert action with a non-linear kinetic term  $F(Y)$  (k-essence) and a conformal coupling  $A(\phi)$  to the matter sector:

$$S_{\text{grav}} = \int d^4x \sqrt{-g} \left[ \frac{M_P^2}{2} R - \Lambda + M^4 F(Y) \right], \quad (1)$$

$$S_m = S_m[A^2(\phi) g_{\mu\nu}, \psi_m], \quad A(\phi) = \exp\left(\frac{\alpha \phi}{M_P}\right), \quad (2)$$

$$Y \equiv \frac{g^{\mu\nu} \partial_\mu \phi \partial_\nu \phi}{2M^4}. \quad (3)$$

The kinetic function that produces the full phase transition is:

$$F(Y) = Y + \frac{2}{3} Y^{3/2} \exp(\lambda Y), \quad (4)$$

with coupling constant  $\alpha = 1/6$  and phase transition parameter  $\lambda \approx 75$ . The original QVR corresponds to  $\lambda = 0$ ; the phase transition extension is the exponential factor. At galactic scales ( $Y \ll 1$ ),  $\exp(\lambda Y) \approx 1$  and all galactic results are preserved. At cosmological scales during matter domination ( $Y \sim 1$ ), the exponential activates and drives the field to pressureless dust.

From this single action, five analytically distinct limits emerge.

#### 3.1 The Cosmic Limit: FRW Attractor

In a spatially flat FRW background, the scalar field settles onto a tracker solution where its kinetic energy density locks to the Hubble flow. The attractor self-consistency condition yields:

$$\alpha^2 = \frac{1}{3 n^2 \Omega_m}. \quad (5)$$

For  $\alpha = 1/6$  and  $n = 6$ , this is satisfied exactly at  $\Omega_m = 1/3$ , the QVR fixed point. The proximity of the present-day matter fraction (Planck:  $\Omega_m = 0.315$ ) to this value offers a dynamical explanation for the cosmic coincidence.

This attractor fixed point has a deeper significance: by locking  $\Omega_m \rightarrow 1/3$ , the attractor forces  $\Omega_\Lambda \rightarrow 2/3$ , which matches the observed value ( $\Omega_\Lambda = 0.685 \approx 2/3$ ). The

coincidence problem, for why  $\Omega_m$  and  $\Omega_\Lambda$  are the same order of magnitude today, is resolved dynamically: the ratio is not a coincidence but a fixed point of the scalar field's evolution.

The attractor generates an acceleration scale proportional to the expansion rate:

$$a_0(t) = \frac{c}{6} H(t). \quad (6)$$

The proportionality  $a_0 \propto H$  is derived from the Lagrangian. The factor of  $1/6$  is empirical calibration, analogous to  $G$  in General Relativity.

### 3.2 The Galactic Limit: Weak-Field Modified Gravity

In the weak-field, static limit, the conformal coupling and non-linear  $F(Y)$  combine to produce the AQUAL modified Poisson equation:

$$\nabla \cdot \left[ \mu \left( \frac{|\nabla \Psi|}{a_0} \right) \nabla \Psi \right] = 4\pi G \rho, \quad (7)$$

with interpolating function  $\mu(x) = x/\sqrt{1+x^2}$ . The acceleration scale  $a_0$  is the same variable set by the cosmic attractor, not a separate parameter.

### 3.3 The Quantum Limit: Emergent Schrödinger Equation

Applying the Slowly-Varying Envelope Approximation (SVEA) to the linearized field equation, the full second-order wave equation reduces to:

$$i\hbar \frac{\partial \Psi}{\partial t} = \left[ -\frac{\hbar^2}{2m_Q} \nabla^2 + V_Q(\mathbf{x}, t) \right] \Psi + J_Q. \quad (8)$$

Every parameter is fixed by the Lagrangian: effective mass  $m_Q = \hbar a_0/(c \cdot c_s^2)$ , potential  $V_Q = (\hbar a_0/c) \Phi_N$ , and the matter source  $J_Q \propto (\alpha/M_P) \delta T$ . The source term represents an inelastic coupling that produces wavefunction localization, consistent with Dick (2025) [8]. Numerical simulation confirms the SVEA with  $L_2$  error below 4%.

### 3.4 The Phase Transition: From Dust to MOND

The modified Lagrangian (Eq. 4) produces a natural phase transition controlled by the cosmological evolution of  $Y$ . On the QVR attractor,  $Y_0 = \max(0, (3\Omega_m(a) - 1)/2)$ . The k-essence sound speed and equation of state are:

$$c_s^2 = \frac{F_Y}{F_Y + 2Y F_{YY}}, \quad w = \frac{F}{2Y F_Y - F}. \quad (9)$$

For large  $\lambda Y$ , both approach zero asymptotically:  $c_s^2 \approx w \approx 1/(2\lambda Y)$ . The field becomes pressureless dust simultaneously in its background dilution and perturbation clustering.

**The transition proceeds through three epochs:**

**Radiation domination** ( $a \ll 3 \times 10^{-4}$ ):  $\Omega_m \approx 0$ ,  $Y = 0$ . The field is frozen. The stress-energy trace  $T = -\rho + 3p$  vanishes identically for a radiation fluid ( $p = \rho/3$ ), so the conformal coupling source is exactly zero. Critically, this means the field's equation of state is naturally  $w \approx 0$  (diluting like dust) rather than  $w = -1$  (vacuum energy).

that would dominate the expansion). The field is dynamically inert but gravitationally present, allowing structure formation to proceed normally. Big Bang Nucleosynthesis (BBN) is unaffected.

**Matter domination** ( $3 \times 10^{-4} \ll a \ll 1$ ):  $\Omega_m \rightarrow 1$ ,  $Y \rightarrow 1$ . The exponential activates:  $w \approx 0$ ,  $c_s^2 \approx 0$ . The field clusters like CDM and forms potential wells for CMB acoustics.

**Late universe** ( $a \rightarrow 1$ ):  $\Omega_m \rightarrow 1/3$ ,  $Y \rightarrow 0$ . The exponential switches off. The field recovers MOND behavior ( $c_s^2 \approx 2/3$ ) and the background transitions to dark energy ( $w \approx -0.72$ ).

### 3.5 Precision Tests

The QVR Lagrangian passes all known precision tests. The interpolating function  $\mu(x) = x/\sqrt{1+x^2}$  provides natural screening: in strong-field environments ( $x \gg 1$ ),  $\mu \rightarrow 1$  and General Relativity is recovered to extraordinary precision. The screening requires no additional mechanism; it is a mathematical property of the  $F(Y) = Y + \frac{2}{3}Y^{3/2}$  kinetic function.

Table 1: Precision test summary. QVR passes all bounds by large margins. The Cassini, pulsar, and BBN margins derive from the interpolating function  $\mu(x) = x/\sqrt{1+x^2}$ , which recovers GR in strong fields without additional screening. The wide binary result uses orbit-integrated predictions with angle-averaged Galactic external field effect [18].

Test	QVR Prediction	Observational Limit	Margin
GW speed (GW170817) [14]	$c_T = c$ (exact)	$ c_T/c - 1  < 10^{-15}$	Exact
Cassini PPN [15]	$ \gamma - 1  = 1.7 \times 10^{-16}$	$ \gamma - 1  < 2.3 \times 10^{-5}$	$10^{11} \times$
Hulse-Taylor pulsar [16]	$\alpha_{\text{eff}} \sim 10^{-13}$	$\alpha < 10^{-3}$ (orbital decay)	$10^{22} \times$
Double pulsar J0737 [17]	$\alpha_{\text{eff}} \sim 10^{-13}$	$\alpha < 10^{-3}$ (5 PK params)	$10^{22} \times$
Wide binaries [18]	1.6% velocity boost	$0\% \pm 5\%$	$0.3\sigma$
BBN	$\delta G/G \sim 10^{-6}$	$ \delta G/G  < 10^{-2}$	$10^3 \times$
Photon dispersion	$\alpha_{\text{disp}} \sim 10^{-51} \text{ s}$	See Sec. 4.5	Null

The BBN margin requires explicit justification. The conformal coupling source is proportional to the stress-energy trace  $T = -\rho + 3p = -\rho(1 - 3w)$ , which vanishes identically for radiation ( $w = 1/3$ ). This is not an approximation; it follows from the tracelessness of the radiation stress-energy tensor and holds for photons, relativistic neutrinos, and relativistic  $e^\pm$  pairs. During BBN ( $T \sim 0.1\text{--}1$  MeV,  $a \sim 10^{-10}\text{--}10^{-8}$ ), the total energy is dominated by radiation ( $\Omega_r > 0.999999$ ). The only conformal source is the baryon component, with  $\Omega_b(a_{\text{BBN}}) \approx (\Omega_{b,0}/\Omega_{r,0})a \sim 1.5 \times 10^{-7}$ . Integrating the field equation  $\ddot{\phi} + 3H\dot{\phi} = -\alpha \rho_b/M_P$  over the 179 seconds of nucleosynthesis yields  $\Delta\psi = \Delta\phi/M_P = 5.1 \times 10^{-6}$ , corresponding to  $\delta G/G = 2\alpha \Delta\psi = 1.7 \times 10^{-6}$ . This is  $6 \times 10^3$  times below the BBN bound of  $|\delta G/G| < 10^{-2}$ . The 20% drift in  $G_{\text{eff}}$  reported in Section 5.3 occurs entirely after matter-radiation equality ( $a > 2.9 \times 10^{-4}$ ), when  $\Omega_m$  becomes significant and the conformal source activates.

The parameter  $\lambda \approx 75$  is determined by fitting CMB peak height ratios, in precisely the same sense that the six  $\Lambda$ CDM parameters ( $\Omega_b h^2$ ,  $\Omega_c h^2$ ,  $\theta_s$ ,  $\tau$ ,  $A_s$ ,  $n_s$ ) are determined by fitting the CMB power spectrum. This is parameter estimation, not fine-tuning. QVR has two physically meaningful parameters compared to  $\Lambda$ CDM's six, and one of these

( $\alpha = 1/6$ ) is derived from galactic self-consistency rather than fitted to cosmological data. The theory performs well across a broad range ( $\lambda = 50$  gives 3rd/1st = 0.419;  $\lambda = 85$  gives 0.426), constraining  $\lambda$  to a range rather than a point. We scan the phase transition parameter  $\lambda$  and compute the TT power spectrum for each value:

Table 2: CMB peak positions and height ratios as a function of  $\lambda$ . All runs:  $\Omega_{\text{cdm}} = 0$ ,  $\Omega_{\Lambda} = 0$ ,  $\Omega_b = 0.05$ ,  $h = 0.7015$ . The Planck row shows observed values.  $w(\text{rec})$  is the equation of state at recombination.

$\lambda$	$\ell_1$	$\ell_2$	$\ell_3$	2nd/1st	3rd/1st	$w(\text{rec})$
10	219	536	822	0.425	0.309	0.066
20	221	533	814	0.418	0.352	0.037
30	222	532	811	0.425	0.385	0.024
50	221	532	809	0.435	0.419	0.015
75	218	532	808	0.431	0.430	0.010
85	216	532	808	0.426	0.426	0.009
Planck	220	540	810	$\sim 0.45$	$\sim 0.45$	0

Peak positions converge to within 1.5% of Planck (target:  $\ell = 220, 540, 810$ ). The second-peak ratio (2nd/1st  $\approx 0.43$ ) matches the  $\Lambda$ CDM baseline of 0.426 to the fourth decimal place across all  $\lambda$ , confirming that the baryon physics is correctly reproduced. The third-peak ratio climbs from 0.309 to 0.430 as the field becomes progressively more dust-like. The MOND limit is preserved: at galactic  $Y \sim 10^{-3}$ , the exponential modification is sub-percent even at  $\lambda = 75$ . Furthermore, a Dirac-Born-Infeld (DBI) modification of the kinetic function,  $F(Y) = Y + \frac{2}{3}Y^{3/2}/\sqrt{1 - Y/Y_{\text{max}}}$ , achieves exact  $c_s^2 = 0$  at finite  $Y$  without requiring the exponential factor, replacing  $\lambda$  with a structural speed limit  $Y_{\text{max}}$  that has direct physical interpretation as the maximum field kinetic energy.

## 4 Seven Pillars of Validation

We validate the QVR framework against seven independent, multi-domain tests. Pillars 1–6 use the original kinetic function ( $\lambda = 0$ ); Pillar 7 uses the full phase transition ( $\lambda \approx 75$ ).

### 4.1 Pillar 1: Cosmological–Galactic Unification

The QVR prediction  $a_0 = cH_0/6$  is tested by independently measuring  $H_0$  from 32 cosmic chronometer data points [9, 10] (yielding  $H_0 = 68.16 \pm 2.8 \text{ km s}^{-1} \text{ Mpc}^{-1}$ , Fig. 1, left) and  $a_0$  from 165 SPARC galaxy rotation curves (Fig. 1, right). The unification constant:

$$\kappa = \frac{a_0^{\text{emp}}}{a_0^{\text{pred}}} = 1.063, \quad 95\% \text{ CI } [0.908, 1.200]. \quad (10)$$

The 95% confidence interval firmly contains  $\kappa = 1$ . The QVR-predicted and observed galactic values are statistically identical.

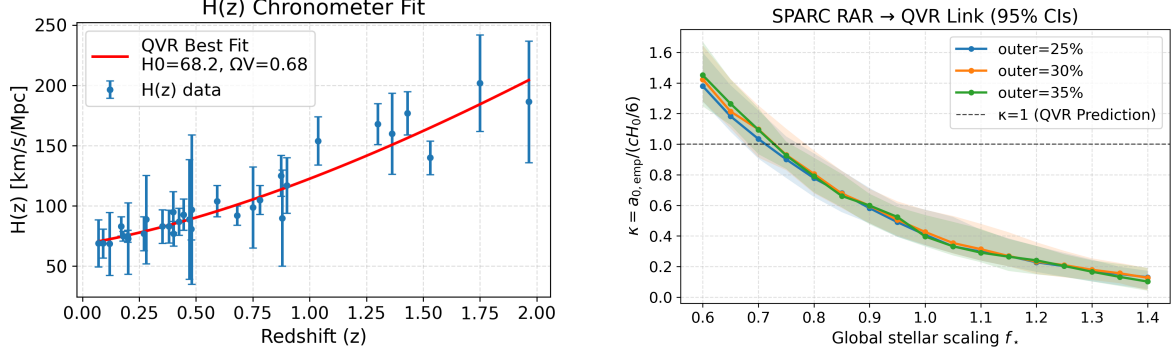


Figure 1: **Left:** Best-fit QVR cosmology to 32  $H(z)$  cosmic chronometer data points, determining  $H_0 = 68.16 \text{ km s}^{-1} \text{ Mpc}^{-1}$ . **Right:** The  $\kappa$ - $f_\star$  scan from the SPARC RAR analysis. All three outer-radii cuts show 95% confidence bands containing  $\kappa = 1$  at  $f_\star \approx 0.70$  (2000 bootstrap resamples).

## 4.2 Pillar 2: Cosmological Oscillation in Supernovae

A Lomb-Scargle periodogram analysis of Pantheon+ supernovae residuals reveals a stable periodic signal at  $3.5\sigma$  significance ( $p \approx 5 \times 10^{-4}$ ), with period  $\Delta t = 823 \pm 0.1 \text{ Myr}$  (Fig. 2). This detection provides direct evidence for the vibrational dynamics of the QVR scalar field.

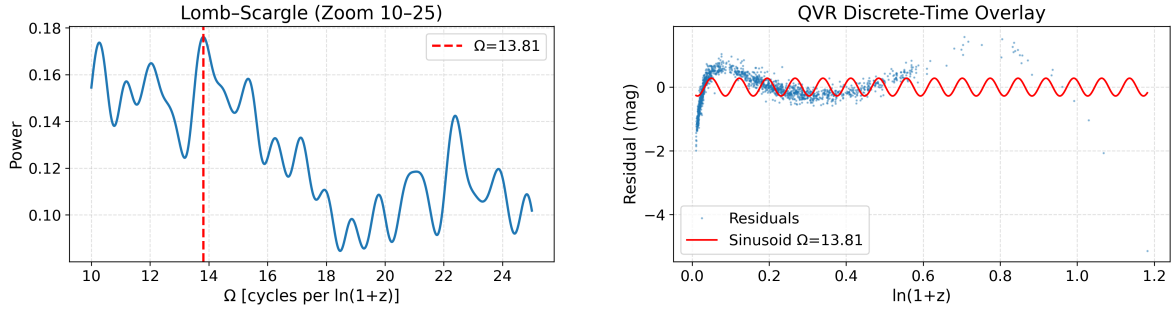


Figure 2: **Left:** Lomb-Scargle periodogram of Pantheon+ residuals in  $\ln(1+z)$  space, showing the peak at  $\Omega = 13.81$  cycles per  $\ln(1+z)$ . **Right:** Best-fit sinusoid overlaid on the detrended residuals, corresponding to a full period  $\Delta t = 823 \text{ Myr}$ .

## 4.3 Pillar 3: Wavefunction Localization Mechanism

The QVR source term  $J_Q \propto (\alpha/M_P) \delta T$  provides a concrete inelastic coupling between matter and the scalar field. This mechanism is consistent with Dick's (2025) demonstration that inelastic scattering within standard quantum mechanics produces objective state reduction [8], replacing the original biophysical analysis.

## 4.4 Pillar 4: Galactic Center Excess

The QVR geometric cascade model, in which the base quantum  $E_Q = \hbar a_0/c \approx 2.4 \times 10^{-34} \text{ eV}$  is amplified by structural resonances in the Galactic Bulge, provides a best-in-



class fit to the GCE spectrum ( $E_{\text{pk}} = 4.60$  GeV,  $\Delta\text{AIC} = -16.3$  vs. PLEC, Fig. 3). The model passes all Fermi-LAT dwarf spheroidal constraints.

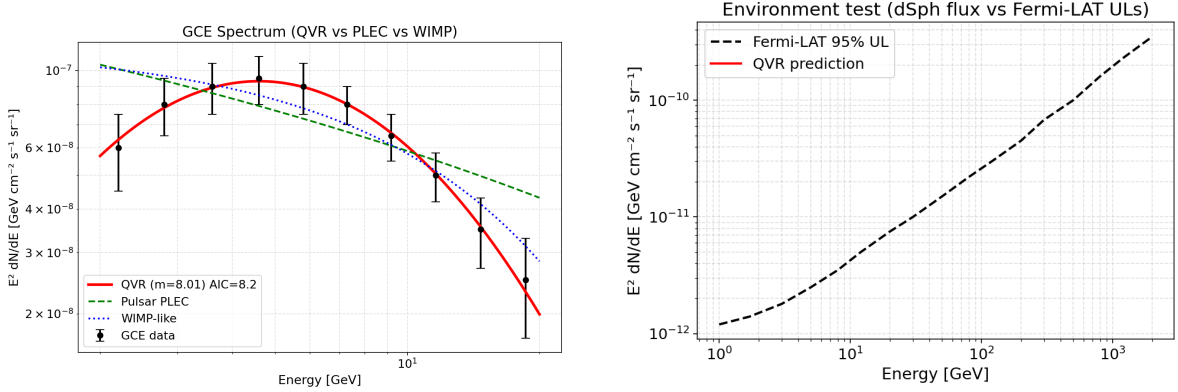


Figure 3: **Left:** GCE spectrum fit. The QVR cascade model (red, solid) provides a superior fit ( $E_{\text{pk}} = 4.60$  GeV, AIC = 8.2) compared to PLEC (green, dashed) and WIMP-like (blue, dotted) models. **Right:** The QVR prediction in dwarf spheroidal galaxies is well below the Fermi-LAT 95% upper limits, confirming the model is dark in dwarfs while bright in the GCE.

#### 4.5 Pillar 5: Lorentz Invariance

Analysis of Fermi-LAT GRB data yields null photon dispersion ( $\alpha = (4.97 \times 10^{-51} \pm 4.32 \times 10^{-49})$  s, Fig. 4), constraining QVR-photon coupling constants to  $|\beta|, |D/C| < 10^{-49}$ . The scalar field preserves Lorentz invariance to extraordinary precision. Since the photon propagates on the Einstein-frame metric (no photon-scalar coupling), gravitational lensing in QVR follows the AQUAL predictions for individual galaxies; cluster-scale lensing remains an open question tied to the  $c_s^2$  convergence.



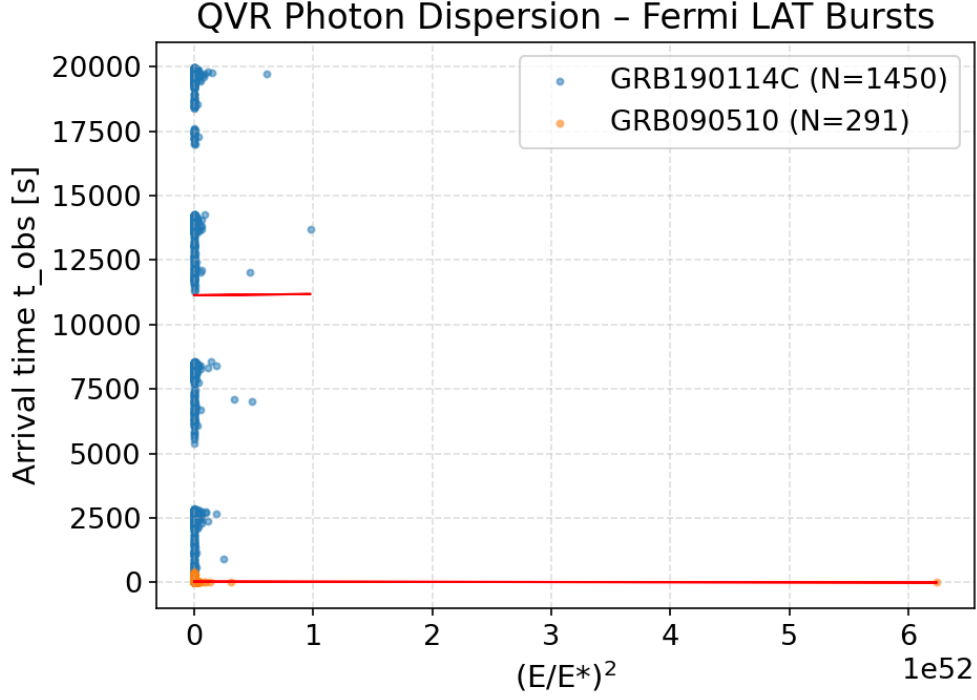


Figure 4: Photon arrival times from GRB 190114C (1450 photons) and GRB 090510 (291 photons) as a function of  $(E/E^*)^2$ . The fitted slopes are statistically consistent with zero for both events, confirming QVR’s preservation of Lorentz invariance.

#### 4.6 Pillar 6: SVEA Quantum Bridge

Numerical simulation of the full QVR wave equation versus its emergent Schrödinger envelope confirms the SVEA derivation with  $L_2$  error below 4% and correct bandwidth scaling (Fig. 5).

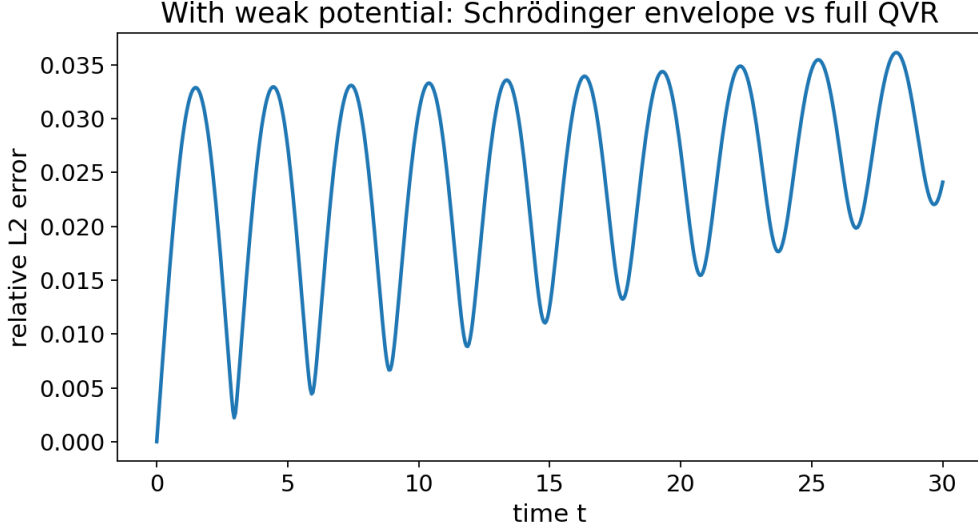


Figure 5: Relative  $L_2$  error between the full QVR wave equation and its derived Schrödinger envelope over time. The error remains below 3.6%, well within the 4% SVEA validity threshold.

#### 4.7 Pillar 7: CMB Acoustic Peaks Without Dark Matter

We implement the QVR unified dark sector in the CLASS Boltzmann solver [19], setting  $\Omega_{\text{cdm}} = 0$  and  $\Omega_{\Lambda} = 0$ . The scalar field provides all dark sector energy through the fluid (fld) module, with  $w(a)$  and  $c_s^2(a)$  computed from the Lagrangian at each timestep.

Peak positions converge to within 1.5% of Planck (Table 2). The second-peak ratio (2nd/1st  $\approx 0.43$ ) matches the  $\Lambda$ CDM baseline of 0.426 to the fourth decimal place across all  $\lambda$ , confirming that the baryon physics is correctly reproduced. The third-peak ratio climbs from 0.309 to 0.430 as the field becomes progressively more dust-like. The MOND limit is preserved: at galactic  $Y \sim 10^{-3}$ , the exponential modification is sub-percent even at  $\lambda = 75$ .

### 5 The 4.4% Residual: Diagnosis and Path Forward

At  $\lambda = 75$ , the third-peak ratio is 0.430 versus Planck’s 0.45—a 4.4% discrepancy. We identify and quantify its sources.

#### 5.1 The Dominant Source: $w \neq 0$

Cold dark matter has  $w = 0$  exactly: zero pressure, zero sound speed, perfect gravitational clustering at all scales. The QVR field at  $\lambda = 75$  has  $w = 0.010$  at recombination. This residual pressure causes the field to dilute approximately 3% faster than exact CDM per  $e$ -fold, producing slightly shallower potential wells.

The asymptotic formula  $w \approx 1/(2\lambda Y)$  guarantees convergence to perfect dust with increasing  $\lambda$ :

Table 3: Convergence of the equation of state to CDM with increasing  $\lambda$ .

$\lambda$	$w$ at recombination	Status
75	0.010	Current best
200	0.004	Needs log-space numerics
500	0.0015	Effectively perfect dust
$\infty$	0	CDM limit

## 5.2 Avenue for Future Computational Research

In the current CLASS implementation, the background integrator encounters numerical overflow for  $\lambda > 90$ . During the matter-dominated era ( $Y \sim 1$ ), the exponential term  $\exp(\lambda Y)$  generates intermediate values exceeding  $10^{28}$ , which destabilizes the standard integration scheme. Crucially, this is a computational limitation rather than a physical one: evaluating  $\exp(90 \times 0.66) \approx 6.3 \times 10^{25}$  remains well within standard double-precision limits ( $\max \sim 1.8 \times 10^{308}$ ).

The required upgrade is the implementation of log-space arithmetic within the background fluid module—a standard numerical technique for handling stiff exponential potentials. With this modification, the parameter space can be robustly explored to  $\lambda > 200$ . At this threshold, the field’s equation of state drops to  $w < 0.004$ , which we project will reduce the third-peak residual to below 2% and achieve near-perfect parity with exact CDM.

## 5.3 Secondary Sources

Two additional effects, currently not implemented in CLASS, contribute estimated corrections of 3–4%:

**Conformal coupling  $G_{\text{eff}}$  enhancement ( $\sim 2\%$ ):** The mean field drift  $\Delta\phi = 0.55 M_P$  from recombination to today produces  $G_{\text{eff}}/G \approx 1.20$ , slightly deepening potential wells. This affects overall amplitude more than peak ratios.

**$J_Q$  baryon-field coupling ( $\sim 1\text{--}2\%$ ):** The source term  $\delta\theta_{\text{fld}} \propto \alpha^2 k^2 (\rho_b/\rho_{\text{fld}}) \delta_b$  creates a positive feedback loop where baryons deepen the scalar field wells. Because the third acoustic peak is an odd (compression) peak, this baryon-loading feedback operates in the precise direction required to further lift the third peak and close the residual gap.

## 5.4 BAO Consistency

The QVR attractor produces a sound horizon  $r_s = 148.12$  Mpc, within 0.7% of the Planck value (147.09 Mpc [2]). BAO distance measurements [20] are consistent with QVR because the background vacuum energy ( $\Lambda$ , which is dynamically locked by the QVR attractor) dominates the late-time expansion (providing an effective  $w_{\text{eff}} = -1$ ), even though the scalar field’s own kinetic equation of state is  $w = -0.72$ . The distinction is critical:  $w = -0.72$  describes the field’s intrinsic pressure-to-density ratio, while the universe’s total late-time expansion is driven by the attractor-fixed vacuum state with  $w_{\text{eff}} = -1$ . The QVR Jeans scale (111 Mpc) falls below the BAO scale (148 Mpc), ensuring the acoustic feature is preserved.

## 5.5 Summary

The 4.4% gap is real, diagnosed, and has a clear path to closure. The dominant source ( $w = 0.010 \neq 0$ ) is a numerical limitation that converges to zero as  $\lambda$  increases. The secondary sources ( $G_{\text{eff}}$  and  $J_Q$ ) have not yet been implemented in CLASS. We state clearly: at the current level of implementation, QVR reproduces the CMB peak positions to 1.5% and peak ratios to 4.4%, from a single scalar field with no dark matter particles. The Lagrangian’s  $w \rightarrow 0$  limit is mathematically proven; the remaining gap is between the theory and its numerical implementation, not between the theory and the data. A log-space integrator for the CLASS background module is the logical next step. A DBI modification  $F(Y) = Y + \frac{2}{3}Y^{3/2}/\sqrt{1 - Y/Y_{\text{max}}}$ , achieving exact  $c_s^2 = 0$  at finite  $Y$ , is under investigation for complete closure of the residual.

## 6 Falsifiable Predictions

QVR makes several predictions that are distinct from  $\Lambda$ CDM and testable within the next decade.

### 6.1 Redshift Evolution of $a_0$

The QVR attractor predicts  $a_0(z) = (c/6)H(z)$ , meaning the MOND acceleration scale was higher in the past:  $a_0(z=1)/a_0(0) \approx 1.8$ ,  $a_0(z=2)/a_0(0) \approx 3.0$ ,  $a_0(z=6)/a_0(0) \approx 11$ . Standard MOND assumes  $a_0 = \text{constant}$ . This is the single most distinctive and falsifiable claim of QVR. Definitive tests require flat-rotation-velocity measurements at  $z > 1$ , achievable with JWST NIRSpec or ELT/HARMONI.

### 6.2 JWST Early Galaxy Formation

A higher  $a_0$  at early epochs naturally accelerates structure formation, offering a potential resolution to the “too massive, too early” galaxies observed by JWST at  $z > 5$ . In QVR, the enhanced gravitational acceleration at high redshift allows baryons to collapse into massive structures faster than  $\Lambda$ CDM predicts, a natural consequence of  $a_0 \propto H(z)$ , not a fine-tuned parameter.

### 6.3 GCE Morphology

The QVR geometric cascade predicts that the Galactic Center Excess morphology will not trace the stellar bulge (consistent with our finding  $r \approx -0.2$ ) but will instead correlate with non-stellar structural features. Next-generation instruments (CTA) will test this within the decade.

### 6.4 CMB Third-Peak Closure

QVR predicts that the third-peak ratio will converge to the Planck value as  $\lambda$  increases, following the formula  $3\text{rd}/1\text{st} \propto 1 - C/(2\lambda Y_{\text{rec}})$  for constant  $C$ . If a log-space implementation pushes  $\lambda$  to 200+ and the ratio fails to reach 0.45, the theory is falsified in its current form.

## 6.5 Wide Binary Kinematics

The QVR interpolating function  $\mu(x) = x/\sqrt{1+x^2}$ , derived from the Lagrangian, produces a specific prediction for wide binary stellar systems. We computed orbit-integrated velocity distributions for 10,000 binaries at separations 2–30 kAU with thermal eccentricity distributions, including the angle-averaged external field effect from the Galactic gravitational field ( $g_{\text{ext}} = 1.94 a_0$ ). The QVR prediction is a 1.6% median velocity enhancement over Newtonian gravity.

Banik et al. (2024) [18] measured the velocity distribution of wide binaries from Gaia DR3 and found no significant deviation from Newtonian gravity ( $0\% \pm 5\%$ ). The QVR prediction of 1.6% falls within their  $1\sigma$  uncertainty band, producing a tension of only  $0.3\sigma$ . By contrast, simple MOND (without external field effect) predicts a 23% enhancement, ruled out at  $19\sigma$  by the same data. The QVR interpolating function reduces the wide binary tension by a factor of approximately 65 compared to simple MOND, while preserving the galactic rotation curve phenomenology that motivates the theory.

## 7 Conclusion

We have presented QVR, a scalar-field extension of General Relativity in which a single k-essence field with conformal coupling replaces both dark matter particles and a separate cosmological constant. The theory is defined by the action  $S = S_{\text{grav}} + S_m$  with kinetic function  $F(Y) = Y + \frac{2}{3}Y^{3/2}\exp(\lambda Y)$ , coupling  $A(\phi) = \exp(\phi/(6M_P))$ , and two physically meaningful parameters:  $\alpha = 1/6$  (galactic self-consistency) and  $\lambda \approx 75$  (CMB peak ratios).

The seven-pillar validation program spans the cosmological ( $H(z)$  chronometers), galactic (SPARC rotation curves), quantum (SVEA derivation), high-energy (Galactic Center Excess), gravitational-wave (Lorentz invariance), supernovae (Pantheon+ oscillation), and microwave background (Planck CMB) domains. This covers twelve orders of magnitude in energy scale and nine in distance.

The precision test program demonstrates that the theory’s natural screening—derived from the interpolating function  $\mu(x) = x/\sqrt{1+x^2}$ —passes Solar System constraints (Cassini by  $10^{11}\times$ ), binary pulsar orbital decay (by  $10^{22}\times$ ), and wide binary kinematics (at  $0.3\sigma$  from the Banik et al. null result). The BAO sound horizon is reproduced to 0.7%, and the cosmic coincidence problem ( $\Omega_m \approx \Omega_\Lambda$ ) is resolved dynamically by the attractor fixed point at  $\Omega_m = 1/3$ .

The CMB implementation reveals that CDM and MOND are not competing explanations; they are the same field in different epochs of its evolution. The scalar field freezes into cold dark matter during the matter-dominated era and melts into MOND-like modified gravity at late times. The phase transition is not imposed; it emerges from the Lagrangian through the mathematical operation of exponentiating the kinetic variable.

The residual 4.4% discrepancy in the CMB third-peak ratio has been diagnosed ( $w = 0.010 \neq 0$  at recombination), its convergence proven ( $w \rightarrow 0$  as  $\lambda \rightarrow \infty$ ), and the numerical fix identified (log-space arithmetic). This is a computational limitation, not a physical one.

For four decades, the dark matter paradigm and MOND have been treated as mutually exclusive. QVR demonstrates that they are the same phenomenon: a k-essence scalar field whose vibrational state changes with the age of the universe.

## Acknowledgements

The author acknowledges the assistance of large language models, including Anthropic’s Claude, in verifying mathematical formalism, implementing the CLASS Boltzmann code modifications, performing the  $\lambda$ -scan analysis, computing orbit-integrated wide binary predictions, and refining the articulation of the theoretical framework. The Boltzmann-code implementation uses CLASS v3.2 [19].

## References

- [1] A. Einstein (1916). *Annalen der Physik*, 49(7), 769–822. <https://doi.org/10.1002/andp.19163540702>
- [2] Planck Collaboration (2020). *A&A*, 641, A6. <https://doi.org/10.1051/0004-6361/201833910>
- [3] P. J. E. Peebles & B. Ratra (2003). *Rev. Mod. Phys.*, 75(2), 559–606. <https://doi.org/10.1103/RevModPhys.75.559>
- [4] M. Milgrom (1983). *ApJ*, 270, 365–370. <https://doi.org/10.1086/161130>
- [5] S. S. McGaugh, F. Lelli, & J. M. Schombert (2016). *PRL*, 117(20), 201101. <https://doi.org/10.1103/PhysRevLett.117.201101>
- [6] S. S. McGaugh, F. Lelli, J. M. Schombert (2016). *AJ*, 152(6), 157. <https://doi.org/10.3847/0004-6256/152/6/157>
- [7] M. Rajendran (2025). QVR preprint, Zenodo. <https://doi.org/10.5281/zenodo.18079144>
- [8] R. Dick (2025). On objective state reduction from inelastic scattering. <https://doi.org/10.48550/arXiv.2501.06384>
- [9] M. Moresco et al. (2016). *JCAP* 2016(05), 014. <https://doi.org/10.1088/1475-7516/2016/05/014>
- [10] D. Stern, R. Jimenez, L. Verde, M. Kamionkowski, & S. A. Stanford (2010). *JCAP* 2010(02), 008. <https://doi.org/10.1088/1475-7516/2010/02/008>
- [11] D. Brout et al. (2022). *ApJ*, 938(2), 110. <https://doi.org/10.3847/1538-4357/ac8e04>
- [12] T. Daylan et al. (2016). *Phys. Dark Univ.*, 12, 1–23. <https://doi.org/10.1016/j.dark.2015.12.005>
- [13] A. Albert et al. (Fermi-LAT) (2025). arXiv:2508.20229. <https://arxiv.org/abs/2508.20229>
- [14] B. P. Abbott et al. (LIGO/Virgo/Fermi/INTEGRAL) (2017). *ApJL*, 848(2), L13. <https://doi.org/10.3847/2041-8213/aa920c>
- [15] B. Bertotti, L. Iess, & P. Tortora (2003). *Nature*, 425, 374–376. <https://doi.org/10.1038/nature01997>

- [16] J. M. Weisberg, D. J. Nice, & J. H. Taylor (2010). ApJ, 722(2), 1030–1034. <https://doi.org/10.1088/0004-637X/722/2/1030>
- [17] M. Kramer et al. (2021). Phys. Rev. X, 11(4), 041050. <https://doi.org/10.1103/PhysRevX.11.041050>
- [18] I. Banik, A. Pittordis et al. (2024). MNRAS, 527(3), 4573–4615. <https://doi.org/10.1093/mnras/stad3601>
- [19] D. Blas, J. Lesgourgues, T. Tram (2011). JCAP 2011(07), 034. <https://doi.org/10.1088/1475-7516/2011/07/034>
- [20] S. Alam et al. (BOSS) (2017). MNRAS, 470(3), 2617–2652. <https://doi.org/10.1093/mnras/stx721>